ADAPTIVE SPECTRAL REFLECTANCE RECOVERY USING SPATIO-SPECTRAL SUPPORT FROM HYPERSPECTRAL IMAGES

Zohaib Khan, Faisal Shafait and Ajmal Mian

School of Computer Science and Software Engineering
The University of Western Australia

ABSTRACT

Accurate knowledge of spectral reflectance is crucial for hyperspectral image analysis. We propose a novel spectral reflectance recovery method by adaptive spatio-spectral support. The proposed technique is evaluated in both simulated and real illumination scenarios. A multi-illuminant hyperspectral scene database has been collected and made publicly available. Experiments show that the adaptive illuminant estimation reduces the mean angular error of recovered spectra by 13%.

***Index Terms*—** Spectral reflectance, spatio-spectral, hyperspectral image, illumination recovery

1. INTRODUCTION

The appearance of a scene changes with the spectrum of ambient illumination [1]. The human visual system has an intrinsic capability of recognizing colored objects under different illuminations [2]. In machine vision systems, it is desirable to remove the effect of illumination, so as to measure the true spectral reflectance of the objects in a scene[3]. This is because in object detection, segmentation [4] and recognition [5], an illumination invariant view of the object is critical to achieving accurate results [6]. The problem is generally known as *spectral reflectance recovery*.

Hyperspectral imaging is gaining profound interest in medicine, art and archeology, and computer vision [7, 8, 9, 10]. Prior research in spectral reflectance recovery is directed towards trichromatic images [11, 12, 13, 14, 15], which is generally referred to as color constancy. These techniques recover spectral reflectance by processing the image band by band (red, green and blue). However, the bands of a hyperspectral image are highly correlated and the neighboring bands have the potential to contribute to accurate estimation of spectral reflectance. We call the spatial relationship between spectrally neighboring bands as the *spatio-spectral support*.

In this paper, we propose a novel method to adaptively recover spectral reflectance from hyperspectral images using spatio-spectral support. We estimate spectral reflectance based on two important properties of hyperspectral images, correlation between the nearby bands and apriori identification of illuminant type from the image. We show that the adaptive use of spatio-spectral support significantly improves spectral reflectance recovery from hyperspectral images over the classical color constancy methodology.

This research was supported by ARC Grant DP110102399.

2. ADAPTIVE SPECTRAL REFLECTANCE ESTIMATION

The formation of a hyperspectral image $I(x, y, \lambda), \lambda = 1, 2, ..., N$ of a scene is mainly dependent on three physiological factors i.e. the illuminant spectral power distribution (SPD) $L(x, y, \lambda)$, the scene spectral reflectance $S(x, y, \lambda)$, and the system response $C(x, y, \lambda)$ which combines both the sensor spectral sensitivity $q(x, y, \lambda)$ (quantum efficiency) and the filter transmission $F(\lambda)$ such that $C(x, y, \lambda) = q(x, y, \lambda)F(\lambda)$. Considering the illumination and the sensor spectral sensitivity to be spatially invariant, one can concisely represent them as $L(\lambda)$ and $C(\lambda)$

$$I(x, y) = \int_{\lambda} L(\lambda)S(x, y, \lambda)C(\lambda)d\lambda \,. \tag{1}$$

The illuminant spectra can be independently estimated from each band of a hyperspectral image by a parameterized estimation function [12]

$$\hat{L}(\lambda : n, p, \sigma) = \frac{1}{\kappa} \int_y \int_x \left\| \nabla^n I_\sigma(x, y) \right\|_p dx\, dy, \tag{2}$$

where n is the order of differential, $\|.\|_p$ is the Minkowski norm and σ is the scale of the Gaussian filter such that $I_\sigma(x, y) = I(x, y) * G(x, y : \sigma)$ is the gaussian filtered image. The parameter κ is a constant, valued such that the estimated illuminant spectra has a unit ℓ_2 norm.

Spatio-spectral information in hyperspectral images is useful for improving spectral reproduction and restoration [16, 17]. Equation (2) estimates illuminant power by first or higher order statistics of the pixels in each band. We define a *spatio-spectral support*, where each spectral band $I(x, y, \lambda_i)$ is supported by the neighboring bands $I(x, y, \lambda_{i-\omega...,i+\omega})$, where $\omega = 0, 1, 2, ...$ is the spectral

support width. It is so called because the bands are spatially collated in the spectral dimension. An illumination estimate using spatio-spectral support can be presented as

$$\hat{L}(\lambda : n, p, \sigma) = \frac{1}{\kappa} \int_y \int_x \left\| \nabla^n I_\sigma^{\lambda_\omega}(x, y) \right\|_p dx\, dy \quad (3)$$

where $I^{\lambda_\omega} = \{I^{\lambda_0}, I^{\lambda_{\pm 1}}, ..., I^{\lambda_{\pm \omega}}\}$ is the set of neighboring bands, forming the spatio-spectral support as shown in Figure 2. Furthermore, it is intuitive to form a weighted spatio-spectral support such that the nearby bands carry more weight, whereas the bands farther away bear proportionally lesser weights with respect to the distance from the central band. Thus, by introducing weighting, the spatio-spectral support is updated as $I^{\lambda_\omega} = \{w_0 I^{\lambda_0}, w_1 I^{\lambda_{\pm 1}}, ..., w_\omega I^{\lambda_{\pm \omega}}\}$. A standard normal function is applied to weight the spatio-spectral support.

Figure 1 shows SPD of some common illumination sources, both artificial and natural. It can be observed that some illuminant are highly differentiable from others based on their SPD pattern. These SPDs can be broadly categorized into smooth or spiky. Most illumination sources generally exhibit smooth SPD (e.g. daylight) where the spectral power gradually varies across consecutive bands. This implies that illumination estimated from neighboring bands is strongly related and can provide an improved illumination estimate. In contrast, for spiky illumination sources (e.g. fluorescent), the spectral power undergoes sharp variation in certain bands. Therefore, the illumination estimated from nearby bands are weakly related.

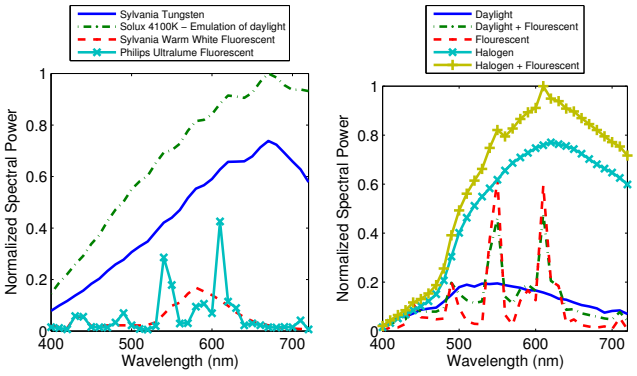

Fig. 1. [Color online] SPD of the illuminations in simulated and real data. Illuminants in SFU data to generate simulated scenes of CAVE data (left). Illuminants measured in the real scenes of UWA data (right). Observe the diversity of illumination spectra in both cases.

To exploit this illumination differentiating characteristic, we devise an adaptive illumination estimation approach. First, an initial estimate of the illumination in a hyperspectral image is achieved using Equation (2). Then, to detect whether the scene is lit by a smooth or a spiky illumination source,

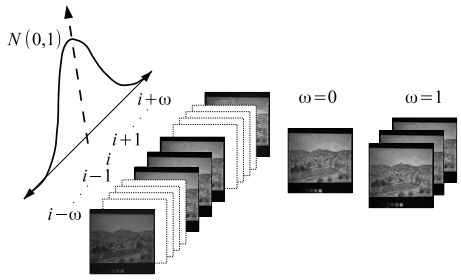

Fig. 2. Structure of spatio-spectral supports of band i for different instants of ω. The spatio-spectral support is weighted by a standard normal distribution function.

this initial estimate is fed to a classifier. The classification is performed by a linear Support Vector Machine (SVM) which is trained on a set of illumination sources labeled as smooth or spiky. If the illumination is classified as smooth, the information in neighboring bands is used for an improved illumination estimate using (3).

Generally, a simplified linear transformation is used to recover spectral reflectance from a hyperspectral image.

$$\hat{I}(x, y, \lambda) = M\, I(x, y, \lambda), \quad (4)$$

where $M \in \mathbb{R}^{N \times N}$ is a diagonal matrix such that

$$M_{i,j} = \begin{cases} 1/\hat{L}(\lambda_i) & \text{if } i = j \\ 0 & \text{otherwise} \end{cases} \quad (5)$$

The *angular error* [18] is a widely used metric for evaluating recovery error. The angular error is defined as the angle between the estimated illuminant spectra $(\hat{L})$, and the ground truth illuminant spectra (L)

$$\epsilon = \arccos\left(\frac{L \cdot \hat{L}}{\|L\|\|\hat{L}\|}\right). \quad (6)$$

The angular error (ϵ) (in degrees) is used for evaluation in this work.

Although, a number of algorithms can emanate by sophisticated instantiations of the parameters (n, p, σ), we restrict our scope only to the widely accepted algorithms in the literature [19, 20] given in Table 1.

Table 1. Methods from different instantiations of parameters in Equation (2)

Methods	n	p	σ
Gray World (GW) [21]	0	1	0
White Point (WP) [22]	0	∞	0
Shades of Gray (SoG) [23]	0	4	0
general Gray World (gGW) [21]	0	9	9
1st order Gray Edge (GE1) [12]	1	1	6
2nd order Gray Edge (GE2) [12]	2	1	1

3. EXPERIMENTAL SETUP

3.1. Imaging Setup

The hyperspectral image acquisition setup is illustrated in Figure 3. The system consists of a monochrome machine vision CCD camera from *Basler Inc.* with a native resolution of 752×480 pixels (8-bit). In front of the camera is a focusing lens (*Fujinon* 1:1.4/25mm) followed by a *VariSpec Inc.* liquid crystal tunable filter, operable in the range of 400-720 nm. The average tuning time of the filter is 50 ms. The filter bandwidth, measured in terms of the *Full Width at Half Maximum (FWHM)* is 7 to 20nm which varies with the center wavelength. The scene is illuminated by a choice of different illuminations.

Figure 4(a) shows the real hyperspectral images rendered as RGB. It can be observed that the rendered images are not visually similar in appearance to RGB images captured by a standard digital camera with white balancing shown in Figure 4(b). This is because the LCTF has low transmission at shorter wavelengths and high transmission at longer wavelengths. Due to this factor, there is more red illuminant power and the resulting images exhibit a reddish tone.

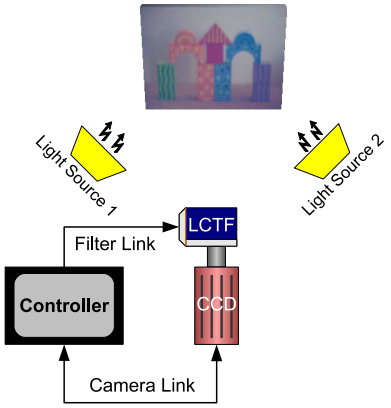

Fig. 3. [Color online] The proposed LCTF based hyperspectral image acquisition setup.

3.2. Dataset Specifications

3.2.1. Simulated Data

The hyperspectral images of simulated illumination scenes are synthesized from the publicly available CAVE multispectral image database[1] which contains true spectral reflectance images. It has 31 band hyperspectral images (420-720nm with 10nm steps) of 32 scenes at a resolution of 512×512 pixels. Each image has a color checker chart in place, masked out to avoid bias in illuminant estimation. The Simon Fraser University (SFU) hyperspectral dataset [24] contains SPDs of 11 real illuminants in (*Set A*) and 81 real illuminants in (*Set B*). We make use of the *Set A* illuminants to simulate lighting scenarios for the images in the CAVE database. The *Set B* illuminants are used to train the SVM to classify an unknown illuminant as smooth or spiky.

[1]CAVE Multispectral Image Database
www1.cs.columbia.edu/CAVE/projects/gap_camera/

3.2.2. Real Data (UWA Multi-illuminant Hyperspectral Scene Database)

Using the imaging setup described previously, we collected a hyperspectral image dataset of real world scenes. The UWA Multi-illuminant Hyperspectral Scene Database contains different scenes captured under five real illumination sources namely daylight, halogen, fluorescent, and two mixed illumination sources, daylight-fluorescent and halogen-fluorescent. Each hyperspectral image has 33 bands in the range (400-720nm with 10nm steps). To create spatially and spectrally diverse scenes, we selected blocks of various shape and color, arranged to form three distinct structures.

(a) Hyperspectral images with non-uniform illumination

(b) RGB images captured with a standard digital camera

Fig. 4. [Color online] Hyperspectral scenes in the UWA database captured by different methods.

4. RESULTS

The angular error distributions for all algorithms are presented in the form of a boxplot[2] (see Figure 5). The results are without the adaptive spatio-spectral support. We observe that the gGW algorithm achieves the lowest mean angular error (MAE). Analysis of the edge based color constancy algorithms GE1 and GE2 indicates that the first order derivative assumption holds better compared to the second order derivative. Overall, GW, WP, SoG and gGW exhibit comparable performances with slight variation.

We now analyze the effect of introducing the adaptive spatio-spectral support. We define relative MAE as the improvement in the mean angular error after introduction of

[2]Boxplot: On each box, the central mark is the median, the lower and upper edge of the box are the 25th and 75th percentiles, respectively. The whiskers extend to the most extreme data points not considered outliers, and the outliers are plotted individually as red crosses. Two medians are significantly different at the 5% significance level if their intervals do not overlap. Interval endpoints are the extremes of the notches.

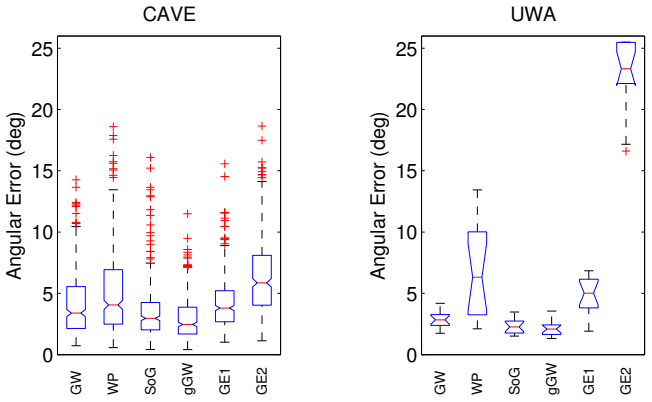

Fig. 5. [Color online] Distribution of angular errors in simulated and real datasets. Observe that the GW, SoG and gGW algorithms achieve the lowest mean angular errors on both databases.

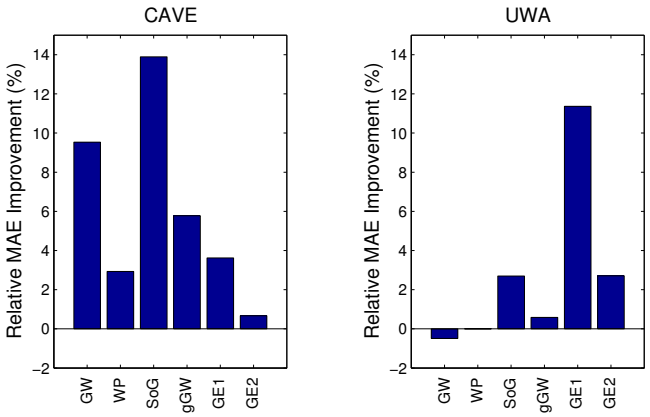

Fig. 6. Relative MAE improvement between non-adaptive and adaptive spatio-spectral support on CAVE and UWA database.

adaptive spatio-spectral support

$$\Delta\bar{\epsilon}_{\text{rel}}\ (\%) = \frac{\bar{\epsilon}_{\text{nad}} - \bar{\epsilon}_{\text{adp}}}{\bar{\epsilon}_{\text{nad}}} \times 100\ . \tag{7}$$

where $\bar{\epsilon}_{\text{nad}}$ and $\bar{\epsilon}_{\text{adp}}$ are the mean angular errors of non-adaptive and adaptive illuminant estimation respectively. A positive $\Delta\bar{\epsilon}_{\text{rel}}$ indicates a decrease in the MAE (i.e. improvement), by adaptive spatio-spectral support and vice versa. Figure 6 shows the relative MAE improvement for all algorithms. It can be observed that the algorithms show up to 13% improvement after the introduction of adaptive spatio-spectral supports on the UWA and CAVE datasets. The superiority of adaptive spatio-spectral support is consistently demonstrated in most algorithms with different degrees of improvement. One can deduce that the parametric assumptions of these algorithms is supportive for smooth illuminant estimation when the information from neighboring bands is integrated. In some instances, the adaptive spatio-spectral support brings no improvement. This is because a mixed illumination source with a dominant smooth component may be misclassified as spiky which is devoid of spatio-spectral support.

We also qualitatively analyze the color constancy results for the sample images shown in Figure 7. The advantage of the adaptive approach is visually appreciable and numerically prominent. Even for the failing algorithm (WP) on an image, the adaptive approach still recovers better illumination estimate and results in lower angular error. Observe the high illumination bias in the real illuminant images compared to the simulated illuminant ones, whereas the illumination is accurately recovered by adaptive spatio-spectral support.

5. CONCLUSION

We proposed a novel method for accurate recovery of spectral reflectance from a hyperspectral images. The adaptive spectral reflectance estimation exploits the spatio-spectral support in hyperspectral images. Experiments were performed on an in house developed and a publicly available database of a variety of objects in simulated and real illumination conditions. It was observed that the identification of the illuminant a priori, is particularly useful for estimating illuminant sources with a smooth spectral power distribution. The adaptive measure for reflectance recovery from spiky illumination scenes is an area worth exploring and our database is publicly available for future research.

The UWA Multi-illuminant Hyperspectral Scene Database: http://www.sites.google.com/site/zohaibnet/Home/databases.

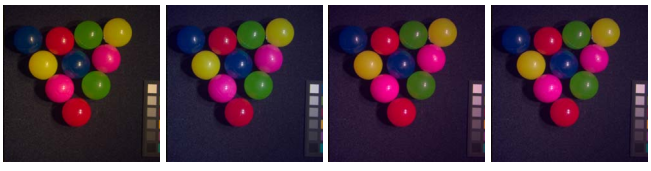

(a) Orig 18.8° (b) Ideal 0° (c) WP 15.7° (d) WP-a 9.9°

(a) Orig 44.5° (b) Ideal 0° (c) SoG 2.3° (d) SoG-a 1.9°

Fig. 7. [Color online] (a) Original image with illumination bias (b) Ideal recovery based on ground truth. Recovery with (c) Non adaptive and (d) Adaptive spatio-spectral support

6. REFERENCES

[1] Jürgen Golz and Donald IA MacLeod, "Influence of scene statistics on colour constancy," *Nature*, vol. 415, no. 6872, pp. 637–640, 2002.

[2] Edwin H Land, *The retinex theory of color vision*, Scientific America., 1977.

[3] Jaka Katrašnik, Franjo Pernuš, and Boštjan Likar, "A method for characterizing illumination systems for hyperspectral imaging," *Optics express*, vol. 21, no. 4, pp. 4841–4853, 2013.

[4] Michael H Brill, "Image segmentation by object color: a unifying framework and connection to color constancy," *JOSA A*, vol. 7, no. 10, pp. 2041–2047, 1990.

[5] Glenn Healey and David Slater, "Global color constancy: recognition of objects by use of illumination-invariant properties of color distributions," *JOSA A*, vol. 11, no. 11, pp. 3003–3010, 1994.

[6] Karl R Gegenfurtner, "Cortical mechanisms of colour vision," *Nature Reviews Neuroscience*, vol. 4, no. 7, pp. 563–572, 2003.

[7] C.M. Wang, C.C.C. Chen, Y.N. Chung, S.C. Yang, P.C. Chung, C.W. Yang, and C.I. Chang, "Detection of spectral signatures in multispectral MR images for classification," *IEEE Transactions on Medical Imaging*, vol. 22, no. 1, pp. 50–61, 2003.

[8] A. Calcagni, J.M. Gibson, I.B. Styles, E. Claridge, and F. Orihuela-Espina, "Multispectral retinal image analysis: A novel non-invasive tool for retinal imaging," *Eye*, vol. 25, no. 12, pp. 1562–1569, 2011.

[9] S. Baronti, A. Casini, F. Lotti, and S. Porcinai, "Principal component analysis of visible and near-infrared multispectral images of works of art," *Chemometrics and Intelligent Laboratory Systems*, vol. 39, no. 1, pp. 103–114, 1997.

[10] A. Pelagotti, A. Del Mastio, A. De Rosa, and A. Piva, "Multispectral imaging of paintings," *IEEE Signal Processing Magazine*, vol. 25, no. 4, pp. 27–36, 2008.

[11] B. Li, W. Xiong, W. Hu, and O. Wu, "Evaluating combinational color constancy methods on real-world images," in *Proc. Computer Vision and Pattern Recognition*, 2011, pp. 1929–1936.

[12] J. Van De Weijer, T. Gevers, and A. Gijsenij, "Edge-based color constancy," *IEEE Transactions on Image Processing*, vol. 16, no. 9, pp. 2207–2214, 2007.

[13] J. Van De Weijer, C. Schmid, and J. Verbeek, "Using high-level visual information for color constancy," in *Proc. International Conference on Computer Vision*, 2007, pp. 1–8.

[14] D.A. Forsyth, "A novel algorithm for color constancy," *International Journal of Computer Vision*, vol. 5, no. 1, pp. 5–35, 1990.

[15] T. Gevers, HMG Stokman, and J. Van De Weijer, "Color constancy from hyper-spectral data," in *Proc. British Machine Vision Conference*, 2000, pp. 292–301.

[16] Yuri Murakami, Ken Fukura, Masahiro Yamaguchi, and Nagaaki Ohyama, "Color reproduction from low-snr multispectral images using spatio-spectral wiener estimation," *Optics express*, vol. 16, no. 6, pp. 4106–4120, 2008.

[17] Ajmal Mian and Richard Hartley, "Hyperspectral video restoration using optical flow and sparse coding," *Optics Express*, vol. 20, no. 10, pp. 10658–10673, 2012.

[18] S.D. Hordley and G.D. Finlayson, "Re-evaluating colour constancy algorithms," in *Proc. International Conference on Pattern Recognition*, 2004, pp. 76–79.

[19] A. Gijsenij, T. Gevers, and J. Van De Weijer, "Computational color constancy: Survey and experiments," *IEEE Transactions on Image Processing*, vol. 20, no. 9, pp. 2475–2489, 2011.

[20] S. Bianco and R. Schettini, "Color constancy using faces," in *Proc. Computer Vision and Pattern Recognition*, 2012, pp. 65–72.

[21] G. Buchsbaum, "A spatial processor model for object colour perception," *journal of the Franklin institute*, vol. 310, no. 1, pp. 1–26, 1980.

[22] E.H. Land, *The retinex theory of color vision*, Science Center, Harvard University, 1974.

[23] G.D. Finlayson and E. Trezzi, "Shades of gray and colour constancy," in *Twelfth Color Imaging Conference: Color Science and Engineering Systems, Technologies, and Applications*, 2004, pp. 37–41.

[24] K. Barnard, L. Martin, B. Funt, and A. Coath, "A data set for color research," *Color Research & Application*, vol. 27, no. 3, pp. 147–151, 2002.